

One Stage Method – Activated Carbon Modified by Surfactant and Irradiation to Highly Improve Adsorption of Lead (II) Ion Wastewater Simulation (Utilization of Banana Peel Biomass)

Dhita Ariyanti^{1,2*}, Deni Swantomo², Asril Pramutadi Andi Mustari¹, Sidik Permana¹

¹ Bandung Institute of Technology, Department of Doctoral Nuclear Engineering, Faculty of Mathematics and Natural Sciences, Ganesha 10 Street, Bandung 40132, Indonesia

² Department of Nuclear Chemical Engineering, Indonesia Polytechnic Institute of Nuclear Technology, National Research and Innovation Agency, Babarsari 60 Street, P.O. Box 6101, Yogyakarta 55281, Indonesia

* Corresponding author's e-mail: dhit001@brin.go.id

ABSTRACT

Banana peel is biomass that can be converted into activated carbon. Changing activated carbon from banana peel biomass would eventually become an innovation, bringing biomass to prominence as a new and renewable energy source. Electromagnetic waves are another approach for activating carbon. Gamma irradiation functions as an ionization agent or initiator, resulting in the production of free radicals. Gamma electromagnetic exposure provides clean energy with no production of chemical components. The purpose of this experiment was to investigate the effect of ⁶⁰Co gamma irradiation on the chemical functional group, surface area, diameter porous formation, and morphology of carbon at 10 to 50 kGy gamma radiation exposure using FTIR, BET, and SEM instrumentation. The results revealed that modification of activated carbon by irradiation and surfactant has a substantial effect on the formation of diameter pores, functional group formation, and porosity structure. The result showed that gamma irradiation exposure significantly affected pore distribution formation on activated carbon because of cellulose decomposition. Gamma irradiation treatment with optimum doses of 30 and 40 kGy on AC/SLS increased the adsorption capacity of Pb²⁺ to 54.31% and 52.67% compared to AC/SLS without irradiation at 41.65%.

Keywords: biomass, activated carbon, surface area, functional groups, adsorption.

INTRODUCTION

Agricultural biomass containing cellulose has good homogeneity with strong acids. Hydrolysis can reduce xylan and degrade complex structures. Most acid compounds are capable of converting cellulose crystals into amorphous ones, including HCl and H₃PO₄ which can remove lignin to activate symmetrical pores. Impregnation with nitric acid can improve the physical properties of activated carbon [1–3]. K₂CO₃ has been proven effective as an activator for agricultural biomass precursors. Carbon is a useful material with numerous benefits, including energy storage applications in batteries, supercapacitors, fuel cells, biosensors,

and drug delivery systems in medicine [1, 2]. Carbon nanomaterials, such as graphene and modified graphene, are also used in water treatment to remove heavy metal ions [3, 4]. On the basis of prior experiments, carbon is a material derived from abundant renewable sources with low exploration costs [5–8]. Various nanocarbons have excellent photoluminescence stability, a broad two-photon absorption area, and functionalization capabilities [9–11]. Furthermore, nanoporous carbon generated from metal-organic frameworks (MOFs) has a very large surface area, allowing it to be used for a variety of applications, including a cation-exchange membrane and a suitable nanofiller for pervaporation membrane matrices

[12–16]. The significant benefit of carbon material motivates researchers to use it in a variety of efficient applications. Meanwhile, carbon must be activated in order to boost its performance. The surface of activated carbon had a large number of active functional sites. Because activated carbon has superior properties to unactivated carbon, it is widely prepared. Better characteristics include increased surface area, well-developed pore shape, superior thermal, adsorption capacity, electrical, and optical properties [15–17].

Activated carbon materials are made using a variety of techniques, including carbonization, hydrothermal processing, pyrolysis, and microwave [17–19]. The activation by chemical and physical substance is the following stage. Carbon activity can be raised by utilizing a variety of chemical substances, such as bases, acids, and salts [19–21]. There are flaws in both approaches. When using the physical activation approach, a significant amount of energy is needed to activate the process. Meanwhile, residual strong acids and bases from the chemical activation process remain present and have an effect on pollution in the environment [19, 20].

In addition to the use of strong acids and bases, surfactants can be used to activate carbon. Surfactants created more active spots on the surface of carbon. In this study, surfactants were applied to the carbon surface to generate SMAC (surfactants modified activated carbon). Gamma irradiation at a specific dose on the material can cause cross-linking. Gamma radiation is electromagnetic radiation produced when unstable atomic nuclei lose energy. Gamma induction initiates the process of chain cross-linking and chain breaking in the polymer matrix. The polymers that are cross-linked can tolerate high-energy gamma radiation at specific doses (1–10 kGy) [47]. Furthermore, cross-linked polymers have excellent qualities, including resilience to high temperatures. In addition to being heat resistant, polymer grafting and composites with gamma radiation induction have good mechanical, thermomechanical, and physiochemical properties [48].

Gamma irradiation of carbon has an influence on both pore and tensile strength [23]. Gamma irradiation of activated carbon was used in treating polymeric materials for high-performance applications [24, 25]. Previous study has suggested that gamma irradiation exposure can be utilized as a modified way to increase carbon performance. Velo Gala *et al.* used gamma to irradiate

activated carbon, and the results revealed that surface carbon hybridization shifted from sp^3 to sp^2 [43]. Terawneh *et al.* found that gamma irradiation improved the mechanical, thermal, and conductivity properties of hybrid carbon nanotubes/montmorillonite nanocomposites [44]. Annisa *et al.* studied the surface modification of nanoporous carbon using gamma irradiation treatment as a supercapacitor material; the results revealed that after irradiation, oxygen functional groups increased and reached an optimal point at a radiation dose of 25 kGy [45]. Degradation of cellulose uses the gamma irradiation mechanism reaction when it contact with the material occurs in two stages. The first stage is the induced ionization process. Temperature of water sample and the humidity of irradiator was about 25.85 °C and 77%. This stage involves the breakage of covalent bonds, which decompose into free radicals. The second stage corresponds to the generated ions that cause chemical interactions between the molecules at varying concentrations. The degradation of gamma irradiation exposure impacts pore formation [36, 42]. From previous work, changing the properties of biomass by different technology used microwave-assisted catalytic pyrolysis of Albizia Branches and Albizia Tree [49, 50]. The novelty in this work is integration of gamma irradiation and surfactant used to change the properties of biomass. The reason of gamma irradiation used because of clean energy, low power, low temperature needed, and no chemical residue release on environmental.

In this study, activated carbon (AC) from banana peel was treated using a surfactant (sodium lauryl sulfate, SLS) and gamma irradiation exposure from ^{60}Co . The goal of this study is to understand how gamma irradiation, as an activator, affects the properties of modified activated carbon. The effect of gamma irradiation exposure was determined using statistical methodologies based on carbon morphological properties.

MATERIALS AND METHODS

Activated carbon material preparation

The approach for altering activated carbon began by cutting banana peel into pieces, which were then sun-dried until dry. The banana peel was then carbonized at 400 °C until carbon was created, which produces smoke. Then it was chilled

in a desiccator, with banana peel being crushed beforehand first. After mashing, it was treated with a salt activator. The activator used was NaCl 60% Merck p.a. Following that, it was allowed to soak for 24 hours. Activated carbon from banana peel was rinsed with distilled water three times before being dried in the oven at 90 °C for \pm 3 hours to reduce humidity and dry the carbon. If the carbon is still damp, it can increase the oven processing time. Furthermore, carbon was treated with 60 ppm sodium lauryl sulfate (SLS) Merck p.a. as surfactants and immersed for 4 hours [17, 18]. The solution was filtered to separate the filtrate from the residue. The residue, in the form of SMAC (surfactant-modified activated carbon) or AC/SLS, would be irradiated. The prepared AC/SLS was placed in various bottles.

Irradiation of AC/SLS with ^{60}Co Gamma Exposure

The synthesized AC/SLS material was bombarded with gamma radiation doses ranging from 10 to 50 kGy ^{60}Co in a gamma irradiator facility at the Polytechnic Institute of Nuclear Technology, National Research and Innovation Agency Yogyakarta in Indonesia. The sample was placed in a sample holder and irradiated with gamma rays. The dose rate for gamma irradiation was 2.2 kGy/h. Thus, to obtain the requisite dose range of 10 to 50 kGy, it must be irradiated at a real-time rate. When the prescribed gamma irradiation dose was reached, the alarm would alert automatically. The specification of Gamma Irradiator is Category I. Gamma irradiators use a radioactive Cobalt-60 source with an energy of 1.17 MeV to 1.33 MeV and a decay time of 5.27 years.

Characterization of carbon material techniques

The functional groups of AC modification were identified using Fourier transform infrared (FTIR) at wavenumber 4000–400 cm^{-1} on a Thermo Scientific Nicolet iS10 in Waltham, MA, USA. The morphological material was examined using a scanning electron microscope (SEM) JEOL JSM-6510LA, Tokyo, Japan, with a voltage of 15 kV. N_2 sorption analysis was performed on the material pores and surface area utilizing a NOVA 2000 analyzer Brunauer Emmet Teller (BET) QuanDiscussiontachrome Inc., Boynton Beach, Florida, USA. The description of BET

measurement was outgas time: 5.0 hrs; analysis time: 89.5 min; outgas temp: 150.0 C; bath temp: 273.0 K; molec. weight: 28.013; cross section: 16.200 \AA^2 ; and liquid density: 0.808 g/cc.

Mechanism of Pb^{2+} adsorption

Filtrate solution from adsorption was pipetted in an amount of 5 ml and placed into a 50 ml measuring flask. Dithizone complexing solution and KCN solution were added and the pH of the solution was adjusted by adding NaOH solution. The absorbance of the sample solution was measured at the maximum wavelength. The concentration of Pb^{2+} in the adsorption filtrate was determined by interpolation into the standard curve or by a linear equation using UV-Visible Spectrophotometry. All the reagents used were Merck p.a.

RESULTS AND DISCUSSION

Chemical functional group of activated carbon by FTIR (fourier transform infrared spectroscopy)

Chemical functional groups were identified using the FTIR method. Figure 1 and Table 1 show the FTIR spectra of activated carbon (AC) from banana peel, non-irradiated surfactant modified carbon (AC/SLS), and irradiated carbon/SLS at various gamma doses. Activated carbon materials can be discovered at peaks about 972.71, 1370.64, 1480.45, 2343.34, 2989.44, and 3201.96 cm^{-1} , representing C-O stretching, C-H bending, C=O stretching, C-H stretching, and O-H stretching [26].

Unirradiated AC/SLS showed peaks at wavenumbers 974.13, 1362.08, 1480.45, 2359.03, 2990.87, and 3209.09 cm^{-1} . The pattern of AC/SLS is similar to that of AC, with an increase in O-H stretching and C-H bending. However, the intensity of the AC/SLS peak at 1362.08 cm^{-1} suggests that C-H bending is sharper than AC. It happened because SLS existed and had C-H bonding. The functional group of O-H stretching is at around 3250–3500 cm^{-1} [27]. In this region, the peak of irradiated AC/SLS gradually decreases. This suggests that when the gamma irradiation dose increases, the functional group of O-H stretching reduces correspondingly.

Table 1 shows that a higher dosage of gamma irradiation leads to a higher normalized

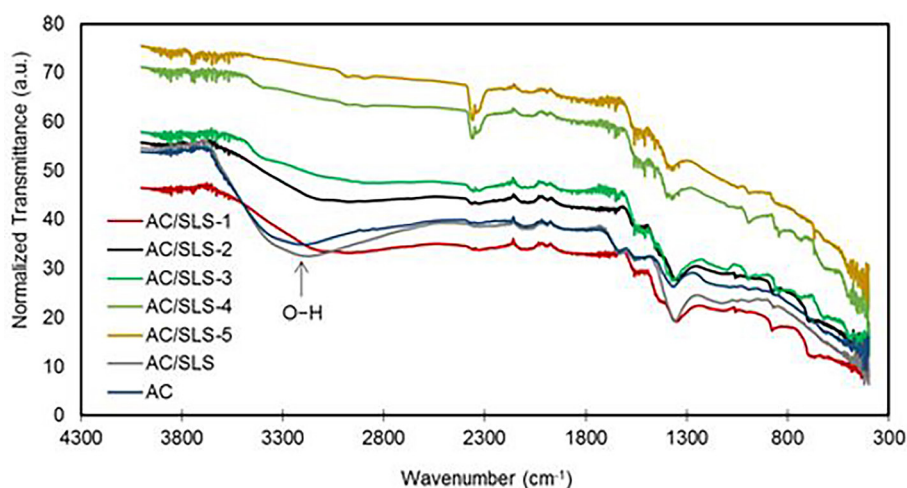


Figure 1. FTIR spectra of from banana peel activated carbon (AC); nonirradiated surfactant modified carbon (AC/SLS); and irradiated AC/SLS at 10 kGy (AC/SLS-1), 20 kGy (AC/SLS-2), 30 kGy (AC/SLS-3), 40 kGy (AC/SLS-4), and 50 kGy (AC/SLS-5)

Table 1. Chemical functional groups of activated carbon materials

Functional group	Wavenumber, cm^{-1} (Normalized Transmittance)						
	AC	AC/SLS	AC/SLS-1	AC/SLS-2	AC/SLS-3	AC/SLS-4	AC/SLS-5
C–O stretching 995–905 [26]	972.71 (25.91)	974.13 (23.52)	976.98 (21.16)	976.98 (28.04)	972.71 (28.62)	952.74 (40.57)	955.59 (45.71)
Skeletal C–C vibrations 700–1300 [28]	1132.45 (26.52)	1132.45 (23.00)	1131.02 (21.47)	1131.02 (28.98)	1128.17 (30.05)	1123.89 (43.50)	1125.32 (48.18)
C–H bending 1365–1380 [26]	1370.64 (26.37)	1362.08 (19.22)	1354.95 (19.19)	1352.10 (27.74)	1362.08 (27.46)	1374.92 (44.07)	1374.92 (50.01)
C=O stretching 2360–1910 [29, 30]						2360.46 (56.57)	2359.04 (60.29)
C–H stretching 2960–2850 [26]	2989.44 (37.08)	2990.87 (34.41)	2995.15 (33.26)	2996.57 (43.75)	2993.72 (48.18)	2993.72 (63.71)	2993.72 (69.53)
O–H stretching 3250–3500 [27]	3201.96 (34.89)	3209.09 (32.64)	3203.38 (35.09)	3203.38 (45.45)	3203.38 (50.12)	3203.38 (65.55)	3203.38 (71.74)

transmittance. AC/SLS irradiated at 10, 20, 30, 40, and 50 kGy resulted in increased transmittance O–H stretching (34.89; 32.64; 35.09; 45.45; 50.12; 65.55; and 71.74 a.u.). This condition occurs when the amount of functional O–H is lowered. This finding is consistent with prior research into the effects of gamma irradiation on certain materials. Phonlam *et al.* (2023) reported that peak characteristics reduce oxygen moieties due to radical production. The creation of $\text{OH}\bullet$ and $\text{H}\bullet$ in this material system could be due to an interaction with the surface of carbon [24].

Stretching of the functional group C=O occurs between 2360 and 1910 cm^{-1} [29, 30]. The AC pattern is identical to both unirradiated AC/SLS and irradiated AC/SLS at 10, 20, and 30 kGy. There is no prominent peak in this region. AC/SLS-4 and AC/SLS-5 have particular peaks at 2360.46 and 2359.04 cm^{-1} , respectively. In

this scenario, a prior study by Walo *et al.* (2018) showed that the effect of gamma irradiation on particular materials can increase the quantity of bonding formation between oxygen and carbon due to radicals. A similar observation was made in this material system, which could be because it reacted with the surface of carbon via double bonding [24, 31].

This revealed that the lower intensity of O–H in 3250–3500 cm^{-1} was due to radical $\text{OH}\bullet$ and $\text{H}\bullet$ forming a carbon-oxygen double bond. The functional group C–H bends at 1365–1380 cm^{-1} . AC/SLS has a sharper peak intensity than the others. It happened because sodium lauryl sulfate was present in the systems. SLS has a methyl ($-\text{CH}_3$) and eleven $-\text{CH}_2$ -s, implying that it contributes to higher C–H bending intensity. In comparison to AC/SLS, irradiated AC/SLS has a lower intensity at any gamma dose. It confirmed

Table 2. Accumulated table of effect gamma dose irradiation on the functional group of activated carbon

Sample	Functional group from FTIR
AC	No functional of C=O, high intensity of O-H and C-H
AC/SLS	No functional of C=O, highest intensity of O-H and C-H
AC/SLS-1	No functional of C=O, higher dose gamma irradiation, lower intensity of O-H and C-H
AC/SLS-2	No functional of C=O, higher dose gamma irradiation, lower intensity of O-H and C-H
AC/SLS-3	No functional of C=O, higher dose gamma irradiation, lower intensity of O-H and C-H
AC/SLS-4	Group C=O, higher dose gamma irradiation, lower intensity of O-H
AC/SLS-5	Group C=O, lowest intensity of O-H and C-H

previous statements by Walo *et al.* (2018), Antonangelo *et al.* (2019), and Phonlam *et al.* (2023) on the formation of OH and H radicals. Similar to the decrease in intensity on the functional group of O-H stretching, decreased C-H bending is caused by radical hydrogen production [24, 26, 31]. Finally, C-C vibrations range from 700–1300 cm^{-1} . The peak in this location is overcrowded due to the high concentration of C-C vibrations in the sample. Activated carbon is made up of numerous heterocyclic rings that are interconnected (Figure 5) [32]. Table 2 resumed effect of gamma irradiation dose on functional group of AC/SLS. FTIR analysis indicates that gamma dose irradiation impacted the reducing O-H and C-H bending functional groups by radical production ($\text{OH}\bullet$ and $\text{H}\bullet$). Gamma dose irradiation increased the strength of the C=O stretching peak (2360-1910 cm^{-1}).

According to a previous study, Antonangelo *et al.* (2019) discovered that this rising peak occurred as a result of the formation of oxygen and the surface of carbon via double bonding (C=O). Table 3 displays an accumulated table showing the effect of gamma dose irradiation on the chemical functional groups or bonds of activated carbon compounds.

Surface area of activated carbon material through Brunauer Emmet Teller

Figure 2 depicts a graph of textural features, focusing on the adsorption isotherms of carbon materials. Activated carbon (AC) from banana peel curve ascended steadily as the relative pressure (P/P_0) increased. According to IUPAC 1985, this isotherm curve may be associated with type II, physical absorption isotherm. The definition of type II physical absorption is gas adsorption using macroporous AC from banana peel as an adsorbent. This type of physical absorption suggests that monolayer-multilayer occurs up to a reasonably high pressure, with multilayer thickness increasing until the relative pressure (P/P_0) equals one [33].

This trend was also observed on irradiated AC/SLS 30 kGy (AC/SLS-3) and 40 kGy (AC/SLS-4). According to the IUPAC 1985 physical absorption isotherm division, unirradiated AC/SLS, irradiation AC/SLS 10 kGy (AC/SLS-1), irradiated AC/SLS 20 kGy (AC/SLS-2), and irradiated AC/SLS 50 kGy (AC/SLS-5) increase according to relative pressure (P/P_0). This shows that the materials (unirradiated AC/SLS, irradiated AC/SLS 10 kGy (AC/SLS-1), irradiated AC/SLS 20 kGy (AC/SLS-2), and irradiated AC/SLS

Table 3. Accumulated table of effect gamma dose irradiation on chemical functional groups or bond of activated carbon materials

Functional group	Discussion about effect gamma dose irradiation on chemical functional groups
C–O stretching [26]	In higher dose of gamma irradiation, the functional group of C–O stretching didn't significantly affect on intensity. The formation of oxygen on surface of carbon via tends to be double bonding, not single bonding
Skeletal C-C vibrations [28]	In higher dose of gamma irradiation, the functional group of C-C vibrations didn't significantly affect on intensity, because there are many C–C heterocyclic rings that are connected to each other in activated carbon systems
C=O stretching [29,30]	In a higher dose of gamma irradiation, the functional group of C=O stretching increases proportionally because of the formation of oxygen and the surface of carbon via double bonding
C–H stretching [26]	In a higher dose of gamma irradiation, the functional group of C–H stretching decreases proportionally because of radical OH^* and H^* formation
O–H stretching [27]	In a higher dose of gamma irradiation, the functional group of O–H stretching decreases proportionally because of radical OH^* and H^* formation

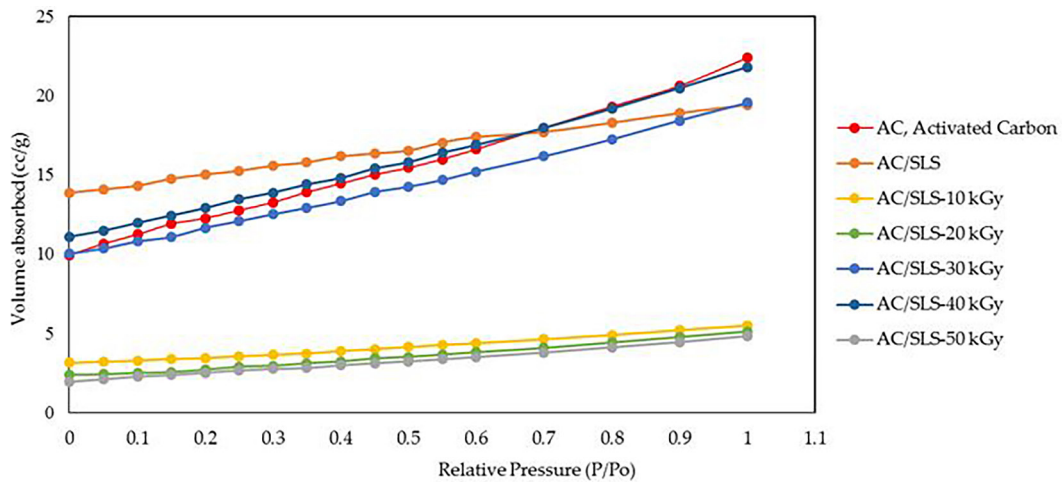


Figure 2. N₂ adsorption isotherms at -196.15°C of activated carbon (AC) from banana peel; nonirradiated surfactant modified carbon (AC/SLS); and irradiated AC/SLS at 10 kGy (AC/SLS-1), 20 kGy (AC/SLS-2), 30 kGy (AC/SLS-3), 40 kGy (AC/SLS-4), and 50 kGy (AC/SLS-5)

50 kGy (AC/SLS-5) are Type I. Type I materials have a broader pore size distribution, including micropores and narrow mesopores [22].

The surface area (SA) graph is shown in Figure 3 and detailed in Table 4. As illustrated in Figure 3, the BET surface area of activated carbon (AC) from banana peel, unirradiated AC/SLS, and irradiated AC/SLS 10 to 50 kGy (AC/SLS-1 to AC/SLS-5) ranges from 7.18 to 41.26 m²/g. Carbon/SLS had the maximum surface area (41.26 m²/g). After gamma irradiation, the maximum surface areas irradiated with AC/SLS 30 kGy (AC/SLS-3) and 40 kGy (AC/SLS-4) are approximately 33.82 and 37.49 m²/g, respectively. Similar to the

preceding explanation, Negara *et al.* (2020) said that a larger BET surface area (m²/g) results in the same sort of physisorption isotherm.

While irradiated AC/SLS at 10 kGy (AC/SLS-1), 20 kGy (AC/SLS-2), and 50 kGy (AC/SLS-5) showed similar physical absorption isotherms. According to the experimental results, the curve of irradiated AC/SLS at 10 kGy (AC/SLS-1), 20 kGy (AC/SLS-2), and 50 kGy (AC/SLS-5) increased along with relative pressure (P/Po). The physisorption isotherm pattern is classified as Type I according to the 1985 IUPAC division. According to the criteria of Type I, irradiated AC/SLS at 10 kGy (AC/SLS-1), 20 kGy (AC/SLS-2),

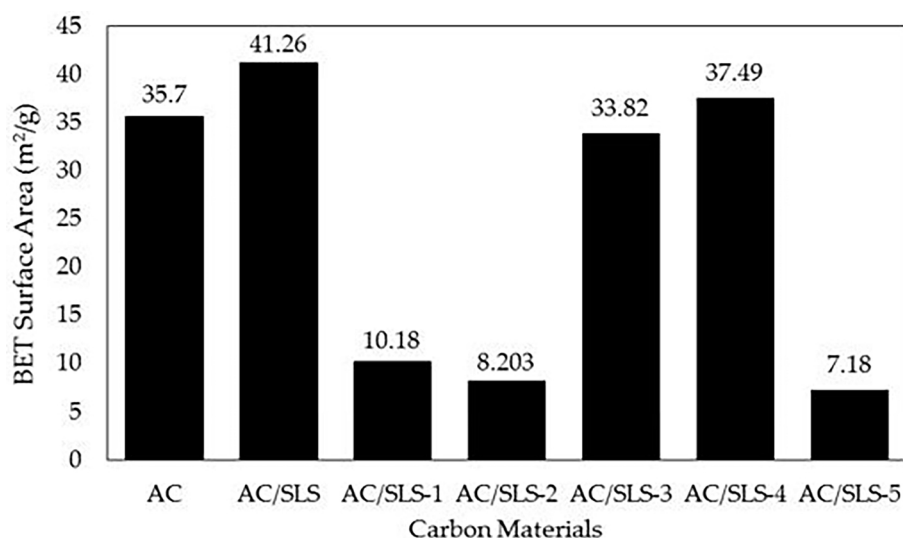


Figure 3. BET surface area (m²/g) of carbon materials

Table 4. BET surface area of carbon materials

Sample	Dose gamma irradiation	BET surface area (m ² /g)
AC	0 kGy	35.70
AC/SLS	0 kGy	41.26
AC/SLS-1	10 kGy	10.18
AC/SLS-2	20 kGy	8.203
AC/SLS-3	30 kGy	33.82
AC/SLS-4	40 kGy	37.49
AC/SLS-5	50 kGy	7.18

and 50 kGy (AC/SLS-5) has a greater range of pore size distribution, including larger micropores and possibly narrow mesopores (< 2.5 nm) [34]. Because of the presence of surfactants, un-irradiated AC/SLS has the largest surface area. Surfactants are chemical compounds that prevent particle aggregation. Because surfactants, in addition to acting as stabilizers in the production of emulsions, coat the produced particles, they limit particle bonding because surfactants have hydrophilic and hydrophobic qualities [35]. The creation of pores occurs in three stages: opening pores, excogitation of new pores, and micropore development. Surfactants cause AC/SLS to develop micropores, rather than macropores.

Irradiated AC/SLS at 10 kGy (AC/SLS-1), 20 kGy (AC/SLS-2), and 50 kGy (AC/SLS-5) have smaller surface areas than irradiated AC/SLS at 30 kGy (AC/SLS-3) and 40 kGy (AC/SLS-4), respectively. This occurred because the degrading process of carbon material by ⁶⁰Co gamma irradiation occluded some holes, resulting in a substantial decrease in surface area [24, 35]. The focus of this research was on optimal dosage gamma irradiation at 30 kGy. This optimal situation is unaffected by the block degradation phenomenon caused by irradiation. In a prior study, Paula *et al.* (2021) reported that sterilization is one of the

consequences of gamma irradiation on material. The mechanical parameters of tensile strength and modulus of elasticity are unaffected by 25 kGy gamma irradiation of PCL (polycaprolactone) films with MCM-48 NPs modified by AP-TES ((3-aminopropyl) triethoxysilane).

Gamma irradiation is an effective approach for sterilizing the material nanocomposite [32, 36–38]. It may be concluded that gamma irradiation exposure has an effect on pore development, as seen by the usual pattern of N₂ adsorption isotherms at -196.15 °C. However, certain irradiated materials have reduced surface areas due to pore blockage during the irradiation process. Table 5 displays the results of the surface area calculation using the ANOVA single-way approach with SPSS IBM. F_{table} or F_{crit} (0.0385) is less than $F_{calculation}$ (4.964), indicating that gamma irradiation had no substantial effect on surface area formation due to pore blockage. Thus, there are two possible conclusions about the influence of gamma irradiation on AC/SLS.

The first is a reduction in surface area due to pore blockage. The second method is gamma irradiation exposure, which is outstanding for sterilizing AC/SLS. SEM photos from the data analysis experiment show that pore formation occurs on surface activated carbon as the dose of gamma

Table 5. Calculation of surface area materials using ANOVA single-way factor

Summary						
Groups	Count	Sum	Average	Variance		
Sample	6	150	25	350		
Surface area (SA)	6	138.133	23.022	258.807		
Anova						
Source of variation	^a SS	^b df	^c MS	^d F	^e p-Value	^f F _{crit}
Between groups	11.735	1	11.735	0.038	0.848	4.965
Within groups	3044.033	10	304.403			
Total	3055.768	11				

Note: ^a sum of Square, ^b degree of freedom, ^c mean squared, ^d analysis of variance, ^e probability-value, ^f F_{criteria}.

irradiation exposure increases. Clearly, this study is entirely based on statistical data, ANOVA. The F significant test shows that gamma irradiation exposure has a significant effect on the distribution of porous diameter development due to $F_{\text{calculation}} > F_{\text{criteria}}$. As a result, the ANOVA statistical test was used to confirm qualitative findings in an experimental setting.

Morphology and pore distribution of activated carbon using scanning electron microscopy

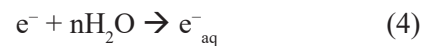
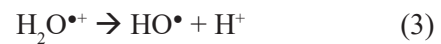
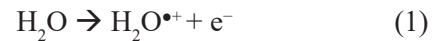
Figure 4 shows the morphology of unirradiated AC (A); irradiated AC/SLS 10 kGy (AC/SLS-1) (B); irradiated AC/SLS 20 kGy (AC/SLS-2) (C); irradiated AC/SLS 30 kGy (AC/SLS-3) (D); irradiated AC 40/SLS kGy (AC/SLS-4) (E); and irradiated AC/SLS 50 kGy (AC/SLS-5) (F). The morphology of the material was characterized via SEM and the distribution porous diameter was analyzed with ImageJ software version 1.52a (64-bit) using ASTM standard E-112 [28].

Table 6 shows the distribution of porosity diameters for each material. Carbon material has an average porosity diameter of 2.05–3.16 μm (derived from Yolanda and Nandiyanto, 2022) [28]. Irradiated AC/SLS 30 kGy has the smallest porous diameter, while irradiated AC/SLS 50 kGy has the largest average porous diameter (F). This finding suggests that gamma irradiation has a considerable effect on the distribution of porous diameter development.

Table 7 displays the significance test results for average diameter porosity (μm) using the ANOVA single-way factor technique via IBM SPSS. As may be observed, F_{table} or F_{criteria} (8.7576) is more than $F_{\text{calculation}}$ (4.964). This finding suggests that gamma irradiation exposure has a significant impact on the diameter of porous development. Polymer grafting, crosslinking, and degradation processes all required an initiator or a chemical agent. In this experiment, radiation gamma ^{60}Co was utilized as an initiator to produce the active site. Gamma radiation has numerous advantages as an initiator, including the fact that it produces no residue, may be utilized at any temperature and in any application, and allows for controlled grafting or degradation. Many researchers have investigated the effects of gamma irradiation on various materials throughout the last decade. Gamma radiation affects a variety of polymer processes. The varied impacts of gamma irradiation dosages

include grafting polymerization, cross-linking, and degradation [33, 39–41, 46].

The way ionizing radiation interacts with the AC, particularly the Compton effect, generates free electrons and positive ions on the AC surface that can react with the water in the irradiation medium. Oxidation reactions are responsible for increasing the surface oxygen concentration. When carbons are exposed to radiation in the presence of water, the gamma radiation interacts with the water molecules as well as the carbon itself, producing (Reactions (1)–(5)) [43].



Radiolysis can modify surface groups, with oxidizing species like HO^{\bullet} causing oxidation and reducing species like H^{\bullet} and e_{aq}^- causing reduction. The FTIR results indicate that the fundamental functional groups (OH stretching, 3200 cm^{-1}) decreased with increasing gamma irradiation dose. It implies that the acid functionalized group increases, although the pH_{zpc} is lower than AC without gamma irradiation treatment. Figure 5 depicts the degradation mechanism response of sodium lauryl sulfate and activated carbon under radiation conditions.

Polymer grafting, crosslinking, and degradation generally need an initiator or chemical agent. In this experiment, radiation gamma ^{60}Co was used to create the active site. The initial stage took place when electrons attacked the surface of activated carbon. The second step in deterioration occurs when the aromatic ring experiences resonance within its ring circle. The movement of double bonds between carbon atoms is known as resonance. The third stage involved shifting electron flow to the closest carbon atoms, which was then followed by the electron resonance process (4th step). The final step was to begin opening cyclic bonds in activated carbon.

Gamma radiation has many benefits as an initiator, including the fact that it produces no residue, may be utilized at any temperature and in any application, and allows for controlled grafting or degradation. Many researchers have investigated the effects of gamma irradiation on materials throughout the last decade. Gamma radiation

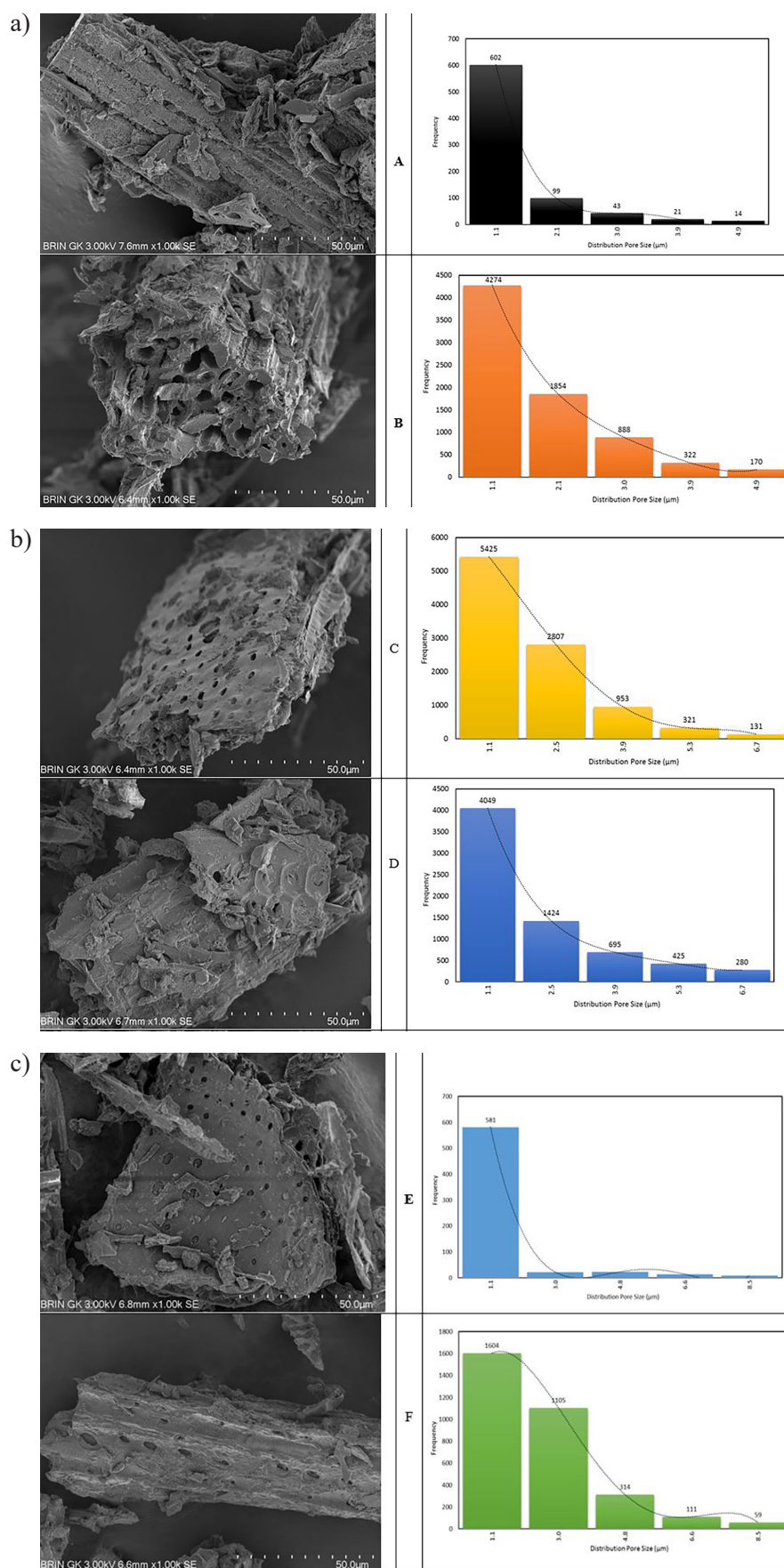


Figure 4. (a) Morphology of unirradiated activated carbon (AC0) (A); irradiated AC 10 kGy (AC1) (B); irradiated AC 20 kGy (AC2); (b) Morphology of irradiated AC 20 kGy (AC2) (C); irradiated AC 30 kGy (AC3) (D); (c) Morphology of irradiated AC 40 kGy (AC4) (E); irradiated AC 50 kGy (AC5) (F)

Table 6. The pore distribution of carbon material was analyzed using ASTM standard E-112

Sample	Average (μm)
AC	2.19
AC1 (10 kGy)	2.18
AC2 (20 kGy)	2.11
AC3 (30 kGy)	2.05
AC4 (40 kGy)	3.16
AC5 (50 kGy)	2.66

affects a variety of polymer processes. Various gamma irradiation doses can have a variety of consequences, including grafting, polymerization, cross-linking, and degradation.

Finally, application on Pb^{2+} adsorption used activated carbon, as shown in Figure 6. On the basis of interpolation data into the standard curve or by a linear equation using UV-Visible Spectrophotometry, the adsorption capacity of Pb^{2+} cations further increased when the activated carbon adsorbent was modified with the addition of SLS surfactant (0.165 mg/gram or 41.65%). This is due to the nature of SLS which is an anionic surfactant with the head part of the surfactant having a negative charge that is able to bind Pb^{2+} cations. The adsorption capacity of Pb^{2+} cations on AC is relatively low because the surface of activated carbon tends to be hydrophobic, while Pb^{2+} cations are hydrophilic species. Hydrophilic species will more easily bind to the species that have the same characteristics. Therefore, the addition of SLS surfactant can increase the adsorption capacity of Pb^{2+} cations because Pb^{2+} cations are more bound to the SLS head which has a sulfonate group.

Gamma irradiation treatment with optimum doses of 30 and 40 kGy on AC/SLS was able to increase the adsorption capacity of Pb^{2+} cations to

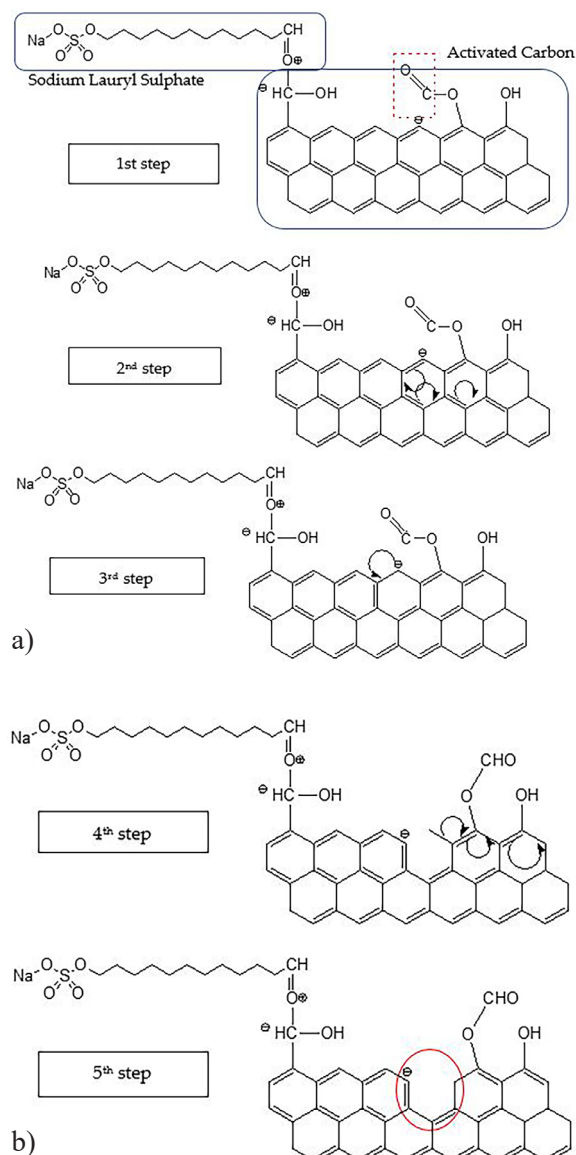


Figure 5. (a) Degradation mechanism reaction of sodium lauryl sulphate and activated carbon on gamma irradiation condition (Step 1 until Step 3); (b) degradation mechanism reaction of sodium lauryl sulphate and activated carbon on gamma irradiation condition (Step 4 and Step 5)

Table 7. Calculation of significance test of average diameter porous (μm) materials using ANOVA single-way factor method

Summary						
Groups	Count	Sum	Average	Variance		
Sample	6	150	25	350		
Average pore diameter	6	14.35	2.392	0.189		
Anova						
Source of variation	^a SS	^b df	^c MS	^d F	^e p-Value	^f F _{crit}
Between groups	1533.41	1	1533.41	8.76	0.014	4.965
Within groups	1750.94	10	175.41			
Total	3284.35	11				

Note: ^a sum of square; ^b degree of freedom; ^c mean squared; ^d analysis of variance; ^e probability-value; ^f F_{crit} criteria.

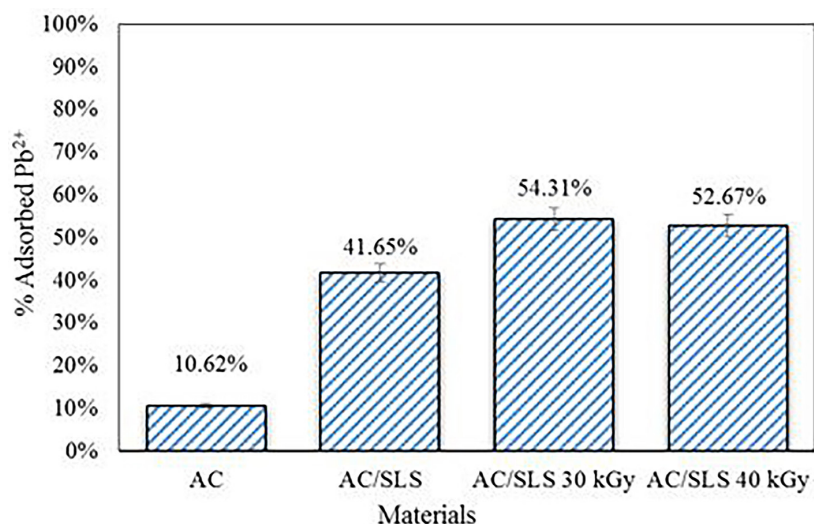


Figure 6. Pb²⁺ adsorption on modified activated carbon (AC) from banana peel

54.31% and 52.67% compared to AC/SLS without irradiation 41.65%. The increase in adsorption capacity is likely due to the large number of active sites on the surface of activated carbon that are activated by exposure to gamma irradiation. This active site then binds to SLS, which then adsorbs Pb²⁺ cations.

CONCLUSIONS

According to the research findings, gamma dose irradiation reduces O-H and C-H bending functional groups due to the generation of OH and H radicals. Gamma dose irradiation increased the C=O stretching peak intensity (2360–1910 cm⁻¹) by forming oxygen and carbon surfaces through double bonding. According to BET characterization, gamma irradiation exposure can impact pore development, as seen by the pattern of N₂ adsorption isotherms at -196.15 °C under normal conditions. Surprisingly, some irradiated samples had a decreased surface area, most likely due to pore blockage during the irradiation procedure; this is confirmed by ANOVA one-way analysis. Gamma irradiation exposure has a considerable impact on the formation of average diameter porous structures (μm). Overall, ⁶⁰Co gamma irradiation at an optimized dose (30 kGy) can impact functional group and porosity formation. Gamma irradiation treatment with optimum doses of 30 and 40 kGy on AC/SLS was able to increase the adsorption capacity of Pb²⁺ cations to 54.31% and 52.67% compared to AC/SLS without irradiation 41.65%.

Acknowledgements

This research was funded by The Research and Community Service Unit, Indonesian Polytechnic Institute of Nuclear Technology for the research and publishing funding.

This manuscript is the only one paper for requirement of first author's on Department of Doctoral Nuclear Engineering, Faculty of Mathematics and Natural Sciences, Bandung Institute of Technology.

REFERENCES

1. Alatzas, S.; Moustakas, K.; Malamis, D.; Vakalis, S. 2019. Biomass potential from agricultural waste for energetic utilization in Greece. *Energies* 12, 95. <https://doi.org/10.3390/en12061095>
2. Kusuma, H.D.; Rochmadi; Prasetyo, I.; Ariyanto, T. 2021. Mesoporous manganese oxide/lignin-derived carbon for high performance of supercapacitor electrodes. *Molecules* 26, 7104. <https://doi.org/10.3390/molecules26237104>
3. Baby, R.; Saifullah, B.; Hussein, M.Z. 2019. Carbon nanomaterials for the treatment of heavy metal-contaminated water and environmental remediation. *Nanoscale Res. Lett.* 14, 341.
4. Ghasemi, M.; Daud, W.R.W.; Hassan, S.H.A.; Oh, S.E.; Ismail, M.; Rahimnejad, M.; Jahim, J.M. 2013. Nano-structured carbon as electrode material in microbial fuel cells: a comprehensive review. *J. Alloys Compd.* 580, 245–255. <https://doi.org/10.1016/j.jallcom.2013.05.094>
5. Ghasemi, M.; Shahgaldi, S.; Ismail, M.; Yaakob, Z.; Daud, W.R.W. New generation of carbon nanocomposite proton exchange membranes in microbial fuel cell systems. *Chem. Eng. J.* 2012, 184, 82–89.

- <https://doi.org/10.1016/j.cej.2012.01.001>
6. Ogunlode, P.; Abunumah, O.; Orakwe, I.; Shehu, H.; Muhammad-Sukki, F.; Gobina, E. 2019. Comparative evaluation of the effect of pore size and temperature on gas transport in nano-structured ceramic membranes for biogas upgrading. *WEENTECH Proc. Energy* 5, 195–205. <https://doi.org/10.32438/wpe.8319>
 7. Zhang, Z.; Zhu, Z.; Shen, B.; Liu, L. 2019. Insights into biochar and hydrochar production and applications: A review. *Energy* 171, 581–598. <https://doi.org/10.1016/j.energy.2019.01.035>
 8. Zheng, X.; Wang, H.; Gong, Q.; Zhang, L.; Cui, G.; Li, Q.; Chen, L.; Wu, F.; Wang, S. 2015. Highly Luminescent Carbon Nanoparticles as Yellow Emission Conversion Phosphors. *Mater. Lett.* 143, 290–293. <https://doi.org/10.1016/j.matlet.2014.12.138>
 9. Chaikittisilp, W.; Hu, M.; Wang, H.; Huang, H.S.; Fujita, T.; Wu, K.C.W.; Chen, L.C.; Yamauchi, Y.; Ariga, K. 2012. Nanoporous carbons through direct carbonization of a zeolitic imidazolate framework for supercapacitor electrodes. *Chem. Commun.* 48, 7259–7261. <https://doi.org/10.1039/c2cc33433j>
 10. Georgakilas, V.; Perman, J.A.; Tucek, J.; Zboril, R. 2015. Broad family of carbon nanoallotropes: classification, chemistry, and applications of fullerenes, carbon dots, nanotubes, graphene, nanodiamonds, and combined superstructures. *Chem. Rev.* 115, 4744–4822. <https://doi.org/10.1021/cr500304f>
 11. Li, X.; Rui, M.; Song, J.; Shen, Z.; Zeng, H. 2015. Carbon and graphene quantum dots for optoelectronic and energy devices: A review. *Adv. Funct. Mater.* 25, 4929–4947. <https://doi.org/10.1002/adfm.201501250>
 12. Marpaung, F.; Kim, M.; Khan, J.H.; Konstantinov, K.; Yamauchi, Y.; Hossain, M.S.A.; Na, J.; Kim, J. 2019. Metal–organic framework (MOF)-derived nanoporous carbon materials. *Chem. An. Asian J.* 14, 1331–1343. <https://doi.org/10.1002/asia.201900026>
 13. Sadeghi Rad, T.; Ansarian, Z.; Khataee, A.; Vahid, B.; Doustkhah, E. 2021. N-doped graphitic carbon as a nanoporous MOF-derived nanoarchitecture for the efficient sonocatalytic degradation process. *Sep. Purif. Technol.* 256, 117811. <https://doi.org/10.1016/j.seppur.2020.117811>
 14. Jirimali, H.; Singh, J.; Boddula, R.; Lee, J.K.; Singh, V. 2022. Nano-structured carbon: its synthesis from renewable agricultural sources and important applications. *Materials* 15, 3969. <https://doi.org/10.3390/ma15113969>
 15. Liu, Y.J.; Liu, S.; Li, Z.W.; Ma, M.G.; Wang, B. 2018. A microwave synthesized mesoporous carbon sponge as an efficient adsorbent for Cr(VI) removal. *RSC Adv.* 8, 7892–7898. <https://doi.org/10.1039/c8ra00012c>
 16. Sun, X.; Liu, Y.; Xu, R.; Chen, Y. 2022. MOF-derived nanoporous carbon incorporated in the cation exchange membrane for gradient power generation. *Membranes* 12, 322. <https://doi.org/10.3390/membranes12030322>
 17. Al-Latief, D.N.; Arnelli, A.; Astuti, Y. 2015. Synthesis of sodium lauryl sulphate (SLS)-modified activated carbon from rice husk for waste lead (Pb) removal. *AIP Conf. Proc.* 1699, 060017. <https://doi.org/10.1063/1.4938371>
 18. Anisyah, A.; Arnelli, A.; Astuti, Y. 2021. SMAC-SLS dari tempurung kelapa menggunakan aktivator ZnCl₂ dan gelombang mikro sebagai adsorbent kation Pb(II). *Greensph. J. Environ. Chem* 1, 1–6.
 19. Liu, Z.; Huang, Y.; Kommentar, G.Z. 2016. Label für nachhaltigen fisch fehlt–wissen–süddeutsche. *BioResources* 11, 3178–3190.
 20. Oginni, O.; Singh, K.; Oporto, G.; Dawson-Andoh, B.; McDonald, L.; Sabolsky, E. 2019. Influence of one-step and two-step KOH activation on activated carbon characteristics. *Bioresour. Technol. Rep.* 7, 100266. <https://doi.org/10.1016/j.biteb.2019.100266>
 21. Hassan, M.; Liu, Y.; Naidu, R.; Parikh, S.J.; Du, J.; Qi, F.; Willett, I.R. 2020. Influences of feedstock sources and pyrolysis temperature on the properties of biochar and functionality as adsorbents: a meta-analysis; Elsevier B.V.: Amsterdam, The Netherlands, 744.
 22. Negara, D.N.K.P.; Nindhia, T.G.T.; Surata, I.W.; Hidayat, F.; Sucipta, M. 2020. Textural characteristics of activated carbons derived from tabah bamboo manufactured by using H₃PO₄ chemical activation. *Mater. Today Proc.* 22, 148–155. <https://doi.org/10.1016/j.matpr.2019.08.030>
 23. Xiao, H.; Lu, Y.; Wang, M.; Qin, X.; Zhao, W.; Luan, J. 2013. Effect of gamma-irradiation on the mechanical properties of polyacrylonitrile-based carbon fiber. *Carbon* 52, 427–439. <https://doi.org/10.1016/j.carbon.2012.09.054>
 24. Phonlam, T.; Weerasuk, B.; Sataman, P.; Duangmanee, T.; Thongphanit, S.; Nilgumhang, K.; Anantachaisilp, S.; Chutimasakul, T.; Kwamman, T.; Chobpattana, V. 2023. Ammonia modification of activated carbon derived from biomass via gamma irradiation vs. hydrothermal method for methylene blue removal. *South Afr. J. Chem. Eng.* 43, 67–78. <https://doi.org/10.1016/j.sajce.2022.10.004>
 25. Naikwadi, A.T.; Sharma, B.K.; Bhatt, K.D.; Mahanwar, P.A. 2022. Gamma radiation processed polymeric materials for high performance applications: A review. *Front. Chem.* 10, 837111. <https://doi.org/10.3389/fchem.2022.837111>
 26. Antonangelo, J.A.; Zhang, H.; Sun, X.; Kumar, A. 2019. Physicochemical properties and morphology of biochars as affected by feedstock sources and pyrolysis temperatures. *Biochar* 1, 325–336. <https://doi.org/10.1007/s42773-019-00028-z>
 27. Keiluweit, M.; Nico, P.S.; Johnson, M.G.; Kleber, M. 2010. Dynamic molecular structure of plant biomass-derived black carbon(biochar)- supporting information. *Environ. Sci. Technol.* 44, 1247–1253.
 28. Yolanda, Y.D.; Nandiyanto, A.B.D. 2021. How to read and calculate diameter size from electron

- microscopy images. *ASEAN J. Sci. Eng. Educ.* 2, 11–36. <https://doi.org/10.17509/ajsee.v2i1.35203>
29. El-Hendawy, A.N.A. 2006. Variation in the FTIR Spectra of a Biomass under Impregnation, Carbonization and Oxidation Conditions. *J. Anal. Appl. Pyrolysis* 75, 159–166. <https://doi.org/10.1016/j.jaap.2005.05.004>
30. Reza, M.S.; Ahmed, A.; Caesarendra, W.; Abu Bakar, M.S.; Shams, S.; Saidur, R.; Aslfattahi, N.; Azad, A.K. 2019. *Acacia holosericea*: An invasive species for biochar, bio-oil, and biogas production. *Bioengineering* 6, 33. <https://doi.org/10.3390/bioengineering6020033>
31. Walo, M. 2018. Radiation-Induced Grafting. In *Applications of Ionizing Radiation in Materials Processing*; Institute of Nuclear Chemistry and Technology: Warszawa, Poland.
32. Thommes, M.; Kaneko, K.; Neimark, A.V.; Olivier, J.P.; Rodriguez-Reinoso, F.; Rouquerol, J.; Sing, K.S.W. 2015. Physisorption of gases, with special reference to the evaluation of surface area and pore size distribution (IUPAC Technical Report). *Pure Appl. Chem.* 87, 1051–1069. <https://doi.org/10.1515/pac-2014-1117>
33. Nowruz, R.; Heydari, M.; Javanbakht, V. 2020. Synthesis of a chitosan/polyvinyl alcohol/activate carbon biocomposite for removal of hexavalent chromium from aqueous solution. *Int. J. Biol. Macromol.* 147, 209–216. <https://doi.org/10.1016/j.ijbiomac.2020.01.044>
34. Ashfaq, A.; Clochard, M.C.; Coqueret, X.; Dispenza, C.; Driscoll, M.S.; Ulański, P.; Al-Sheikhly, M. 2020. Polymerization reactions and modifications of polymers by ionizing radiation. *Polymers* 12, 2877. <https://doi.org/10.3390/polym12122877>
35. Augustine, R.; Saha, A.; Jayachandran, V.P.; Thomas, S.; Kalarikkal, N. 2015. Dose-dependent effects of gamma irradiation on the materials properties and cell proliferation of electrospun polycaprolactone tissue engineering scaffolds. *Int. J. Polym. Mater. Polym. Biomater.* 64, 526–533. <https://doi.org/10.1080/00914037.2014.977900>
36. Erizal, E.; Abbas, B.; Sukaryo, S.G.; Barleany, D.R. 2015. Synthesis and characterization superabsorbent hydrogels of partially neutralized acrylic acid prepared using gamma radiation; swelling and thermal behavior. *Indones. J. Chem.* 15, 281–287. <https://doi.org/10.22146/ijc.21197>
37. Paula, M.V.; de Azevedo, L.A.; de Lima Silva, I.D.; Vinhas, G.M.; Junior, S.A. 2021. Effects of gamma radiation on nanocomposite films of polycaprolactone with modified MCM-48. *Polimeros* 31, 1–10. <https://doi.org/10.1590/0104-1428.20210044>
38. Gueven, O. 2023. An overview of current developments in applied radiation chemistry of polymers. In *Proceedings of the Advances in radiation chemistry of polymers*. IAEATECDOC-1420, IAEA, Notre Dame, IN, USA 13–17 September 33–39.
39. Shinyama, K. 2018. Influence of electron beam irradiation on electrical insulating properties of PLA with soft resin added. *Polymers* 10, 898. <https://doi.org/10.3390/polym10080898>
40. Tamada, M. 2018. Radiation processing of polymers and its applications. in *radiation applications*; Kudo, H., Ed.; Springer: Singapore, 63–80.
41. Reichmanis, E.; Frank, C.W.; O'Donnell, J.H.; Hill, D.J.T. 1993. *Radiation Effects on Polymeric Materials*; Springer International Publishing: Berlin/Heidelberg, Germany.
42. Kudoh, H.; Sasuga, T.; Seguchi, T. 1996. High-energy ion irradiation effects on polymer materials. *ACS Symp. Ser.* 620, 2–10. <https://doi.org/10.1021/bk-1996-0620.ch001>
43. Velo-Gala, I.; López-Peñalver, J.J.; Sánchez-Polo, M.; Rivera-Utrilla, J. 2014. Surface modifications of activated carbon by gamma irradiation. *Carbon* 67, 236–249. <https://doi.org/10.1016/j.carbon.2013.09.087>
44. Tarawneh, M.A.; Sarairah, S.A.; Chen, R.S.; Ahmad, S.H.; Tarawni, M.; Jiun Y.L. 2021. Gamma irradiation influence on mechanical, thermal and conductivity properties of hybrid carbon nanotubes/montmorillonite nanocomposites. *Radiation Physics and Chemistry* 179, 1–11. <https://doi.org/10.1016/j.radphyschem.2020.109168>
45. Annisa, A.; Prasetyo, I.; Swantomo, D.; Ariyanto, T. 2021. Surface Modification of Nanoporous Carbon Using Gamma Irradiation Treatment as Supercapacitor Material 2349, 02000. <https://doi.org/10.1063/5.0052360>
46. Ariyanti, D.; Swantomo, D.; Permana, S.; Pramutadi, A. 2023. Effect of Gamma ⁶⁰Co Irradiation on Morphology of Carbon/Sodium Lauryl Sulphate Using a Novel SEM EDS. *Malaysian Journal of Microscopy* 19, 5, 15–23. <https://malaysianjournalofmicroscopy.org/ojs/index.php/mjm/article/view/705>
47. Fel, E.K. 2016. Comparative Study of Gamma-Irradiated PP and PE Polyolefins Part 2: Properties of PP/PE Blends Obtained by Reactive Processing with Radicals Obtained by High Shear or Gamma-Irradiation. *Polymer* 82; <https://doi.org/10.1016/j.polymer.2015.10.070>, 217–227
48. More, C.V., Alsayed, Z., Badawi, M.S., Thabet, A.A., Pawar, P.P. 2021. Polymeric composite materials for radiation shielding: a review. *Environ. Chem. Lett.* 19; <https://doi.org/10.1007/s10311-021-01189-9>, 2057–2090
49. Maha F.A., Atheer M.A. 2025. The potential significance of microwave-assisted catalytic pyrolysis for valuable bio-products driven from albizia tree. *Applied Sciences and Engineering Process.* 18.01. <https://doi.org/10.14416/j.asep.2024.07.016>
50. Maha F.A., Atheer M.A., Wameath S.A. 2024. Catalytic microwave pyrolysis of Albizia branches using Iraqi bentonite clays. *Iraqi Journal of Chemical and Petroleum Engineering.* 25, 2, <https://doi.org/10.31699/IJCPE.2024.2.16>.